Core-Agnostic Compliance Perception for Rigid–Deformable Coupled Objects using Vision-Based Tactile Sensing

Can Zhao, Yanghui Ding, Haonan Zhao, Yebao Hu and Daolin Ma

***Abstract*—Rigid–deformable coupled objects, such as stone fruits and biological tissues, consist of deformable envelopes enclosing rigid cores. While humans can readily perceive envelope compliance despite internal variations, achieving comparable core-agnostic compliance perception in robots remains challenging. This paper presents a FEM-guided framework for estimating the elastic modulus of deformable envelopes in rigid–deformable coupled objects. The method formulates compliance estimation as a physics-based inverse problem in continuum mechanics and derives a unified finite-element formulation that naturally accommodates variations in the geometry and placement of the internal rigid cores. Leveraging distributed vision-based tactile sensing, the proposed framework enables data-efficient modulus estimation from a single tactile contact frame. Comprehensive simulations and real-world experiments, including non-destructive fruit maturity assessment, demonstrate accurate and robust compliance estimation across diverse core geometries, contact conditions, and loading configurations.**

I. Introduction

Rigid–deformable coupled objects, such as stone fruits and biological tissues, consist of a deformable envelope enclosing a rigid core, as shown in Fig. 1. For these objects, the compliance of the envelope is often the property of interest, as it reflects functional states such as fruit ripeness or tissue condition. However, reliable estimation of the envelope compliance remains challenging because the measured response is easily confounded by the internal rigid structure.

From the sensing perspective, conventional point-wise probing is sensitive to local heterogeneity and contact conditions [1, 2]. Vision-based approaches that combine probing with external observation partially alleviate these issues but typically rely on dense visual markers and are prone to occlusion during contact [3]. In contrast, vision-based tactile sensors are better suited to this problem, as they directly provide dense measurements of boundary deformation and contact force [4, 5]. Existing compliance estimation methods also remain limited. Learning-based methods [6–8] often demand extensive training data, making it difficult to decouple the compliance of the deformable envelope from the influence of the internal rigid core.

In contrast, this work presents a FEM-guided framework for core-agnostic compliance perception. The method integrates distributed tactile measurements with a continuum-mechanics inverse model to recover the elastic modulus of the deformable envelope from a single tactile contact frame. By explicitly incorporating the known internal core geometry in the FEM discretization, it separates core effects from envelope compliance, yielding a physically grounded and data-efficient formulation for modulus estimation across different core geometries and placements. The key contributions of this work are as follows: i) a core-agnostic modeling of rigid–deformable coupled objects, ii) FEM-guided modulus estimation via distributed tactile sensing, and iii) comprehensive validation and application to fruit maturity detection.

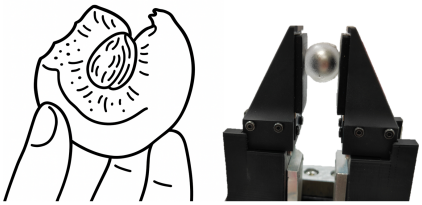

Fig. 1. Compliance perception in rigid–deformable coupled objects. Left: A human pinches a plum to assess envelope compliance. Right: Vision-based tactile sensing enables analogous core-agnostic estimation in robots.

II. Related Work

A. Vision-based Tactile Perception

Tactile perception complements vision in contact-rich manipulation [9], but conventional force/torque sensors and tactile skins are often limited by sparse spatial resolution [10, 11]. Vision-based tactile sensors, represented by GelSight and GelSlim, convert contact-induced membrane deformation into dense visual measurements, enabling high-resolution contact geometry reconstruction [4, 5] and full-field force estimation [12]. Exploiting dense tactile fields to identify mechanical properties of heterogeneous, rigid–deformable coupled objects remains largely unexplored.

B. Compliance Perception for Deformable Objects

Estimating compliance or elastic modulus has long been studied in biomechanics and robotics [1, 13]. Classical indentation methods fit force-displacement curves with idealized contact models, such as Hertzian, flat-punch, or elastic half-space assumptions [2, 14, 15]. External cameras broaden observability [3], but the performance is limited by self-occlusion. Recent tactile learning methods classify hardness or regress material parameters from sensor images [6–8]; however, they remain data-intensive. In contrast, this work explicitly models deformable envelopes with embedded rigid cores and estimates the envelope modulus through a physics-based FEM inverse formulation constrained by distributed tactile measurements.

This work was supported in part by the National Natural Science Foundation of China (NSFC) under Grants No. 12522202, No. 12272220 and No. 124B1038, and in part by Xense Robotics. Can Zhao and Yanghui Ding contributed equally to this work. *(Corresponding author: Daolin Ma).*

C. Zhao, Y. Ding, H. Zhao, Y. Hu and D. Ma are with the School of Ocean & Civil Engineering, Shanghai Jiao Tong University, Shanghai 200240, China (e-mail: can.zhxx, ding-ding, haonanzhao, yebaohu, daolinma@sjtu.edu.cn).

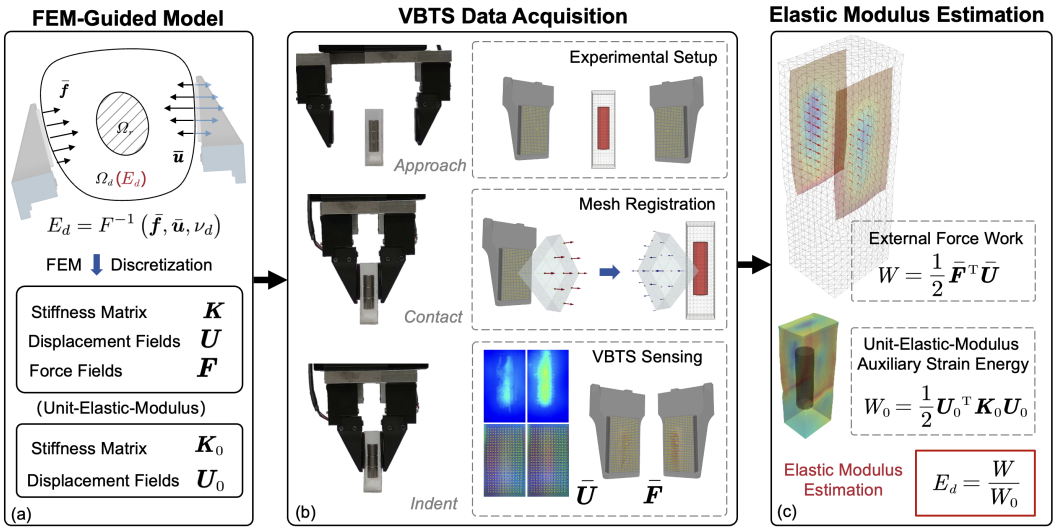

Fig. 2. The overall pipeline. (a) The deformable envelope enclosing a rigid core is discretized using FEM to obtain the unit-modulus stiffness matrix and displacement fields. (b) Vision-based tactile sensors capture full-field deformation during contact, and mesh registration reconstructs boundary displacements and forces. (c) The elastic modulus is estimated by comparing the strain energies of the real and unit-modulus systems.

III. Method

The rigid–deformable coupled object is modeled as a deformable envelope with an embedded rigid core, as shown in Fig. 2. During contact, the tactile sensor measures boundary displacement and force on the contact region. The elastic modulus represents envelope stiffness, and FEM converts the continuous deformable body into a stiffness-matrix relation between nodal forces and displacements.

$$\begin{cases} \boldsymbol{F} = \boldsymbol{K}\boldsymbol{U}, \\ \bar{\boldsymbol{U}} = \boldsymbol{c}^{\text{contact}}\boldsymbol{U}, \bar{\boldsymbol{F}} = \boldsymbol{c}^{\text{contact}}\boldsymbol{F}, \end{cases} \tag{1}$$

where $\boldsymbol{K} \in \mathbb{R}^{n\times n}$ denotes the global stiffness matrix, $\boldsymbol{U} \in \mathbb{R}^n$ and $\boldsymbol{F} \in \mathbb{R}^n$ denote the global nodal displacement and force vectors, $\bar{\boldsymbol{U}} \in \mathbb{R}^m$ and $\bar{\boldsymbol{F}} \in \mathbb{R}^m$ denote the measured nodal displacement and force vectors on contact boundary, and $\boldsymbol{c}^{\text{contact}} \in \mathbb{R}^{m\times n}$ extracts the contact boundary quantities. Here, n is the total number of degrees of freedom, and m is the number of measured contact degrees of freedom. Because the known internal core geometry is explicitly included in the discretization, the effect of the rigid inclusion is handled directly in the mechanical model rather than absorbed into an effective stiffness estimate.

For a linear elastic envelope with fixed Poisson's ratio and a rigid-core constraint, the system matrix can be factorized as $\boldsymbol{K} = E_d\boldsymbol{K}_0$. This separates the unknown envelope modulus E_d from the geometry-dependent part $\boldsymbol{K}_0 \in \mathbb{R}^{n\times n}$. We then solve an auxiliary problem with unit modulus and the same prescribed boundary displacement. The resulting displacement field $\boldsymbol{U}_0 \in \mathbb{R}^n$ is identical to that of the real system, which leads to the closed-form estimator

$$E_d = \frac{\bar{\boldsymbol{F}}^{\mathrm{T}}\bar{\boldsymbol{U}}}{\bar{\boldsymbol{U}}^{\mathrm{T}}\boldsymbol{c}^{\text{contact}}\boldsymbol{K}_0\boldsymbol{U}_0} = \frac{\bar{\boldsymbol{F}}^{\mathrm{T}}\bar{\boldsymbol{U}}}{\boldsymbol{U}_0{}^{\mathrm{T}}\boldsymbol{K}_0\boldsymbol{U}_0}, \tag{2}$$

which can be interpreted as the strain energy ratio between the actual system and a unit-modulus auxiliary system.

IV. Simulation Evaluation

Abaqus simulations provide a controllable testbed for isolating factors that are coupled in real specimens. Two representative interaction modes are considered: a two-sensor grasp of a deformable cuboid with a spherical core and a single-sensor press of a deformable cube with a cubic core, as shown in Fig. 3(a) and (b). The goal is to recover the known envelope modulus while varying one factor at a time. The evaluation focuses on: i) validity of modeling assumptions, ii) advantage of distributed tactile sensing, and iii) the core-agnostic property of the framework.

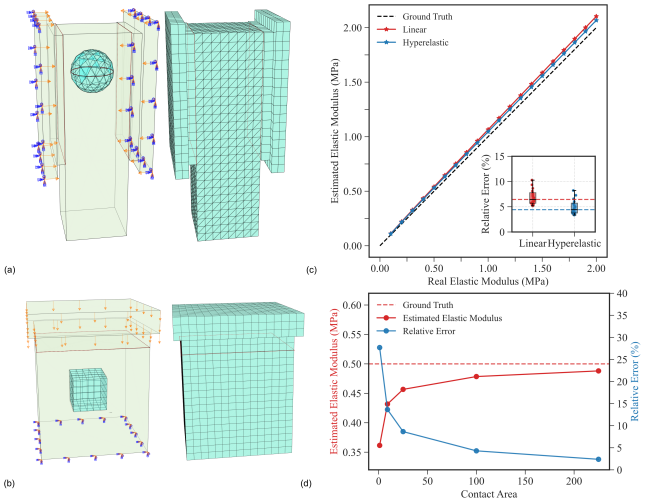

Fig. 3. Abaqus simulation setup and validation. (a) Two-sensor grasp of an object with a spherical core. (b) Single-sensor press of an object with a cubic core. (c) Modulus estimates from linear elastic and Neo-Hookean forward simulations over the tested modulus range. (d) Contact-area sweep in the press case, showing improved accuracy with denser tactile boundary information.

Model Assumption Evaluation. In the grasping case, forward simulations are generated with both a linear elastic model and a Neo-Hookean model, a common nonlinear model, over

the tested modulus range, with other factors fixed. Applying the same estimator to both datasets yields closely matched modulus estimates, as shown in Fig. 3(c), with a maximum discrepancy of 2.01%, indicating limited nonlinear effects.

Tactile Distribution Evaluation. In the pressing case, the contact area is swept over 1^2, 3^2, 5^2, 10^2, and 15^2 mm^2 to evaluate the benefit of distributed tactile measurements. As shown in Fig. 3(d), the estimation error decreases from 27.70% at 1 mm^2 to 8.66% at 25 mm^2, and further drops below 5% at 100 mm^2. This confirms that larger contact area reduces bias caused by local stress concentration and edge effects.

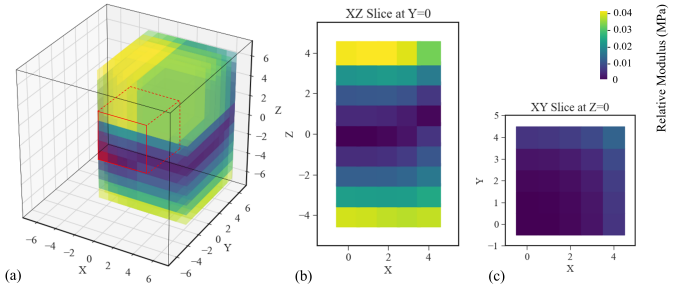

Fig. 4. Sensitivity of modulus estimation to core location. (a) Evaluated core displacement range. Modulus deviation induced by (b) normal-direction perturbations (XZ slice) and (c) tangential perturbations (XY slice).

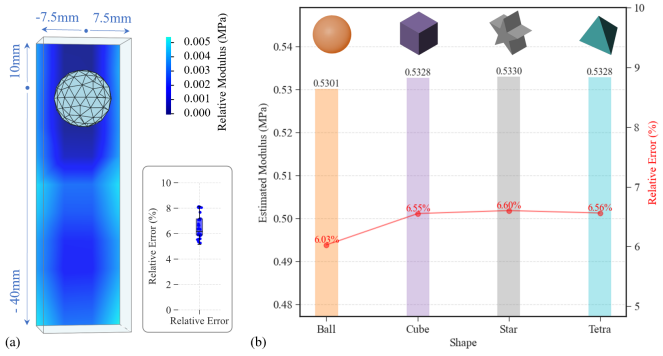

Fig. 5. Core-agnostic evaluation with respect to pressing position and core geometry. (a) Spatial distribution of estimated modulus and relative error across different pressing locations. (b) Estimated modulus and relative error for different core geometries.

Core-Agnostic Evaluation. Core-prior sensitivity is first evaluated by perturbing the assumed core location around its nominal position. Exploiting geometric symmetry, one quarter of the displacement space is sampled using four 1 mm tangential shifts along the x/y directions and normal shifts up to 4 mm along the loading axis, as shown in Fig. 4. The result shows that the estimator is more sensitive to normal than tangential offsets because normal shifts directly change the local envelope thickness along the loading axis. Nevertheless, the maximum error remains within 8%, suggesting tolerance to moderate uncertainty in core placement.

The effects of pressing position and core geometry are then evaluated separately. In Fig. 5(a), the pressing position changes while the core geometry and other factors are fixed. In Fig. 5(b), the modeled core geometry changes among ball, cube, star, and tetrahedral shapes while the pressing condition and core center are fixed. The maximum changes in relative error are 2.97% and 0.57%, respectively, indicating that the estimator is insensitive to these controlled variations.

V. Real-World Experiment

Real-world experiments are conducted to evaluate both controlled modulus estimation and practical fruit compliance perception.

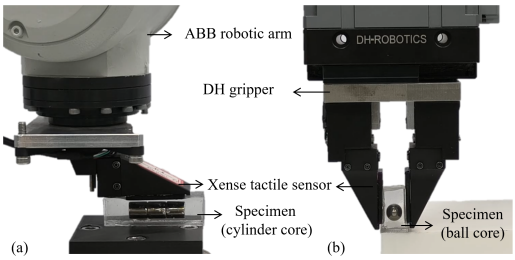

Fig. 6. Real-world experimental setups. (a) Normal pressing with an ABB industrial robotic arm, and (b) grasping with a DH parallel gripper.

TABLE I
Real-world evaluation results of estimated elastic modulus.

Loading & Core Configuration	**Estimated Elastic Modulus** (10^{-2} **MPa**)		
	Cylinder	Ball	Average
Single-sensor Pressing	4.38 ± 0.36	4.29 ± 0.61	4.36 ± 0.43
Two-sensor Grasping	4.63 ± 0.47	4.70 ± 0.31	4.67 ± 0.38
Average	4.41 ± 0.38	4.40 ± 0.56	$\mathbf{4.41 \pm 0.44}$

Controlled experiments on soft PDMS specimens with embedded rigid cores are conducted under single-sensor pressing and two-sensor grasping, using both cylindrical and spherical core geometries, as shown in Fig. 6. The reference modulus is obtained from the same material batch using Shore OO durometer, providing an approximate modulus reference [16]. As shown in Table I, the estimated modulus distributions remain compact across all conditions, with an overall mean relative difference of 3.5% from the Shore-calibrated reference modulus, supporting robustness to both core geometry and loading configuration.

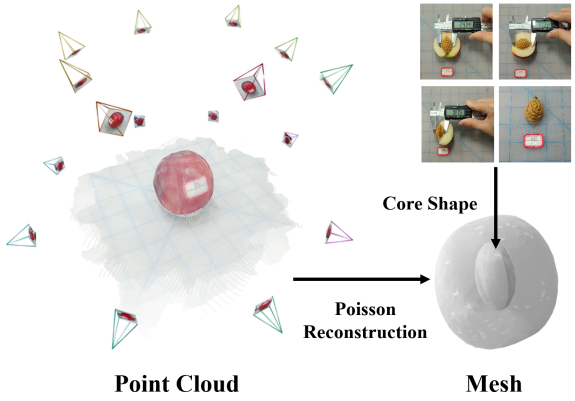

Fig. 7. Fruit geometry reconstruction. A 3D point cloud is generated from multi-view images using VGGT, followed by filtering and Poisson surface reconstruction to obtain a watertight mesh. The core geometry, measured using calipers, is embedded into the reconstructed fruit mesh.

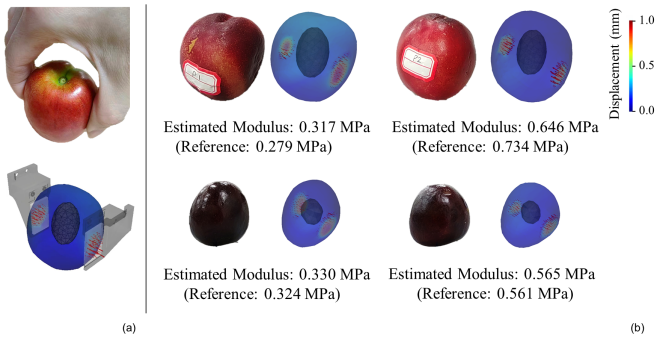

Fig. 8. Fruit modulus estimation. (a) Two-sensor grasping of a fruit. (b) Reconstructed fruit models with embedded pits and displacement fields, with estimated moduli compared against Shore OO references.

The method is further tested on nectarines and cherries with different maturity levels. Because absolute Young's modulus ground truth is not available without destructive mechanical testing, Shore OO hardness is used as a reference trend rather than absolute ground truth. Fruit geometries are reconstructed from multi-view images using the pipeline in Fig. 7. Specifically, VGGT[17], a high-performance visual geometry model, is adopted to generate 3-D point clouds from multi-view images. Scale calibration is performed based on the measured fruit height, followed by point cloud filtering and Poisson surface reconstruction to obtain a watertight mesh. For the internal pit, assuming geometric similarity within the same fruit type, pit dimensions and relative positions are measured from an additional fruit and applied to all fruits of that category. As shown in Fig. 8, the estimated moduli preserve the correct maturity ordering and follow the Shore-based reference trend, supporting non-destructive fruit assessment. This result also highlights a current limitation: pit-size uncertainty mainly perturbs the local envelope thickness along the loading axis, consistent with the core-location sensitivity study.

VI. Conclusion

This paper presents a FEM-guided framework for estimating the elastic modulus of deformable envelopes in rigid–deformable coupled objects based on distributed vision-based tactile sensing. The method can recover the envelope modulus from a single tactile contact frame while explicitly accounting for the effect of the rigid core. This advances tactile material perception beyond homogeneous objects and supports practical non-destructive assessment such as fruit maturity evaluation. Simulations and real-world experiments support robustness to loading configuration, core geometry, and moderate core-placement uncertainty.

A current limitation is that the FEM model still requires an approximate prior on the core geometry, size, and placement; therefore, core-agnostic should not be interpreted as core-free. Core-size uncertainty changes the modeled envelope thickness along the loading path and thus perturbs the unit-modulus strain energy in the energy-ratio estimator. In the fruit experiments, the measured pit is therefore used only as an approximate category-level prior, and the results are interpreted primarily as maturity-related compliance trends. Future work will quantify core-size mismatch and jointly infer core geometry and modulus.

Acknowledgment

This work was supported in part by the National Natural Science Foundation of China (NSFC) under Grants No. 12522202, No. 12272220 and No. 124B1038, and in part by Xense Robotics.

References

[1] W. C. Hayes, L. M. Keer, G. Herrmann, and L. F. Mockros, "A mathematical analysis for indentation tests of articular cartilage," *J. Biomech.*, vol. 5, no. 5, pp. 541–551, 1972.

[2] H. Jin and J. L. Lewis, "Determination of poisson's ratio of articular cartilage by indentation using different-sized indenters," *J. Biomech. Eng.*, vol. 126, no. 2, pp. 138–145, 2004.

[3] T. Xu, M. Li, Z. Wang, Y. Hu, S. Du, and Y. Lei, "A method for determining elastic constants and boundary conditions of three-dimensional hyperelastic materials," *Int. J. Mech. Sci.*, vol. 225, p. 107329, 2022.

[4] W. Yuan, S. Dong, and E. H. Adelson, "Gelsight: High-resolution robot tactile sensors for estimating geometry and force," *Sensors*, vol. 17, no. 12, p. 2762, 2017.

[5] I. H. Taylor, S. Dong, and A. Rodriguez, "Gelslim 3.0: High-resolution measurement of shape, force and slip in a compact tactile-sensing finger," in *Proc. IEEE ICRA*, pp. 10781–10787, IEEE, 2022.

[6] W. Yuan, C. Zhu, A. Owens, M. A. Srinivasan, and E. H. Adelson, "Shape-independent hardness estimation using deep learning and a gelsight tactile sensor," in *Proc. IEEE ICRA*, pp. 951–958, IEEE, 2017.

[7] M. Burgess, J. Zhao, and L. Willemet, "Learning object compliance via young's modulus from single grasps using camera-based tactile sensors," in *Proc. IEEE/RSJ IROS*, pp. 18535–18542, IEEE, 2025.

[8] Z. Li, M. Kuhlmann, I. Nisky, and N. Navarro-Guerrero, "Advances in compliance detection: Novel models using vision-based tactile sensors," *arXiv preprint arXiv:2506.14980*, 2025.

[9] C. Zhao, L. Xie, B. Huang, S. Wang, and D. Ma, "Tactile-driven dexterous in-hand writing via extrinsic contact sensing," *IEEE Robot. Autom. Lett.*, 2025.

[10] W. Lin, B. Wang, G. Peng, Y. Shan, H. Hu, and Z. Yang, "Skin-inspired piezoelectric tactile sensor array with crosstalk-free row+ column electrodes for spatiotemporally distinguishing diverse stimuli," *Adv. Sci.*, vol. 8, no. 3, p. 2002817, 2021.

[11] Z. Pei, Q. Zhang, K. Yang, Z. Yuan, W. Zhang, and S. Sang, "A fully 3d-printed wearable piezoresistive strain and tactile sensing array for robot hand," *Adv. Mater. Technol.*, vol. 6, no. 7, p. 2100038, 2021.

[12] C. Zhao, J. Liu, and D. Ma, "ifem2. 0: Dense 3d contact force field reconstruction and assessment for vision-based tactile sensors," *IEEE Trans. Robot.*, 2024.

[13] R. Martins, J. F. Ferreira, and J. Dias, "Touch attention bayesian models for robotic active haptic exploration of heterogeneous surfaces," in *Proc. IEEE/RSJ IROS*, pp. 1208–1215, IEEE, 2014.

[14] K. L. Johnson, *Contact mechanics*. Cambridge university press, 1987.

[15] C. Zhao, J. Ren, H. Yu, and D. Ma, "In-situ mechanical calibration for vision-based tactile sensors," in *Proc. IEEE ICRA*, pp. 10387–10393, IEEE, 2023.

[16] K. Larson, "Can you estimate modulus from durometer hardness for silicones? yes, but only roughly… and you must choose your modulus carefully," *White paper, Dow Chemical Company*, 2019.

[17] J. Wang, M. Chen, N. Karaev, A. Vedaldi, C. Rupprecht, and D. Novotny, "Vggt: Visual geometry grounded transformer," in *Proceedings of the IEEE/CVF Conference on Computer Vision and Pattern Recognition (CVPR)*, pp. 5294–5306, June 2025.